journal

J. Am. Ceram. Soc., 97 [2] 622–630 (2014)
DOI: 10.1111/jace.12669

Influence of Y and La Additions on Grain Growth and the Grain-Boundary Character Distribution of Alumina

Stephanie A. Bojarski,[‡] Michael Stuer,[§,¶] Zhe Zhao,[¶] Paul Bowen,[§] and Gregory S. Rohrer[‡,†]

[‡]Department of Materials Science and Engineering, Carnegie Mellon University, 5000 Forbes Avenue, Pittsburgh, Pennsylvania 15213

[§]Powder Technology Laboratory, Material Science Institute, Swiss Federal Institute of Technology, Lausanne CH-1015, Switzerland

[¶]Department of Materials and Environmental Chemistry, Arrhenius Laboratory, Stockholm University, Stockholm SE-10691, Sweden

Grain-boundary character distributions (GBCDs) were determined for spark plasma sintered Y- and La-doped aluminas prepared at temperatures between 1450°C and 1600°C. La doping leads to grain boundaries that adopt (0001) orientations 3.7 times more frequently than expected in a random distribution, whereas the Y-doped microstructures are more equiaxed. At 1500°C, some of the boundaries in the Y-doped samples transform to a higher mobility complexion; in this microstructure, the $\{01\bar{1}2\}$ grain-boundary plane is 1.3 times more likely to occur than expected in a random distribution. After the fast-growing grains impinge, the dominant plane becomes $\{11\bar{2}0\}$ and these boundaries have areas that are 1.2 times more likely to occur than expected in a random distribution. The grain-boundary planes in the Y- and La-codoped samples preferred (0001) and $\{01\bar{1}2\}$ orientations, combining the characteristics of the singly doped samples. Grain boundaries with a 60° misorientation about [0001] were up to six times more common than random in the Y-doped samples. The preference for (0001) oriented grain-boundary planes in the La-doped sample persisted at all specific misorientations.

I. Introduction

Yttrium and Lanthanum doping have been shown to significantly increase the creep resistance of polycrystalline alumina.[1–5] Y doping decreases the creep rate of alumina by a factor of two and is more effective than La doping.[1] In both cases, it is known that the dopant cation strongly segregates to the grain boundaries without forming an amorphous intergranular film.[6,7] It is believed that the creep resistance is related to this segregation, but the mechanisms are still not fully understood. In the past, this "Y-effect" has been attributed to changes in grain-boundary diffusivity, solute drag, second phase precipitation, and cation effects on dislocation motion and resistance to grain-boundary sliding.[8] However, the most well supported work in this field shows that a change in the bonding character between the adsorbed Y atoms and the bulk lattice is the most likely cause of these enhanced properties.[2,9,10] It has also been shown that grain-boundary sliding rates depend on the grain-boundary plane orientation, at least for Σ7 grain boundaries.[4] Therefore, both the grain-boundary chemistry and the orientation of the grain-boundary plane may influence creep resistance.

In some investigations, abnormal grain growth (AGG) leading to a bimodal grain size distribution has been seen in the Y-doped alumina samples. It has been shown that ultrapure highly dense Y-doped alumina does not exhibit this abnormal growth.[11] However, when these samples were exposed to Si, whether intentionally doped or contaminated by the processing environment, large equiaxed grains grew abnormally fast.[12] The addition of Si alone has been shown to lead to a highly faceted abnormal grain morphology, so it can be suggested that both Si and Y play a role in the initiation of AGG. Chemical analysis of the abnormal grain boundaries has shown that these abnormal boundaries have a larger amount of Si compared with corresponding normal boundaries, where the total amount of adsorbents is equivalent to roughly a monolayer – as compared with smaller concentrations at normal boundaries.[12] In addition, the amount of Y segregated to alumina grain boundaries has been shown to be proportional to the bulk concentration of Y, up to a specific "super saturation" point, beyond which YAG precipitates are formed that exist in equilibrium with a lower Y concentration.[13,14] In light of more recent developments in the field of grain-boundary kinetics, it is very likely that the Y (Si)-doped alumina system displays a grain-boundary complexion transition that results in increased grain-boundary mobility and AGG.[15]

On the mesoscale, both lanthanum and yttrium doping in alumina have been shown to enhance densification and decrease grain growth of alumina.[11,16] However, in Y-doped alumina sintered above 1550°C, the densification rate decreases and the rate of coarsening increases.[11] In other systems, a change in sintering properties as a function of dopants and thermodynamic variables such as temperature can be attributed to a change in grain-boundary complexion.[15,17] One point of particular interest is the complexion transition that has been reported to occur in Y-doped alumina.[18] As a result of the transition, the grain-boundary mobility increases and the relative grain-boundary energy decreases by 46%.[19] In this work, we will describe the changes in the grain-boundary character distribution (GBCD) that accompany this transition.

There have been many subnanometer to microscale investigations of the grain boundaries in doped aluminas. The limited numbers of boundaries analyzed in each study usually had a special (high symmetry) geometry, so they are not necessarily representative of the bulk of the microstructure.[2,5,7,8,20] There have also been mesoscale studies of similarly doped aluminas by electron backscatter diffraction (EBSD) in which the misorientation angle distributions from

H. Chan—contributing editor

Manuscript No. 33558. Received July 25, 2013; approved September 22, 2013.
†Author to whom correspondence should be addressed. e-mail: gr20@andrew.cmu.edu

many grain boundaries were analyzed.[13,21] However, such analysis does not reveal information about the grain-boundary plane distribution. The purpose of this study was to determine and compare the complete GBCDs, including the grain-boundary plane distributions, in La- and Y-doped alumina. The results show how the dopants influence the grain-boundary populations in alumina, presumably through their influence on the grain-boundary energy.

The GBCD is the relative areas of grain boundaries as a function of the lattice misorientation and grain-boundary plane orientation. Two-dimensional automated EBSD mapping directly determines the three parameters that define the lattice misorientation and one of the two parameters that defines the grain-boundary plane orientation. A stereological technique has been developed to statistically determine the distribution of grain-boundary plane orientations using two-dimensional EBSD maps.[22–24] Because of the stereological relationship between line length per area and grain-boundary area per volume, the five-parameter GBCD in the bicrystal reference frame or the two-dimensional distribution of grain-boundary planes in the crystal reference frame can both be determined from grain-boundary line segments that intersect a surface. While this technique has been used to study grain-boundary populations in many different materials, until now the five-parameter GBCD has not been measured for a trigonal material such as alumina, mainly because the low symmetry of the material increases the number of distinguishable grain boundaries and thus necessitates many observations.

Previous work by Stuer *et al.*[25] investigated the effect of processing variables on the spark plasma sintering (SPS) of Mg, Y, and La-doped alumina. While Stuer's work concentrated on the transparency of fine-grained doped alumina, the current work investigates the grain-boundary character of larger grained opaque samples and focuses more on understanding the effect that Y and La have on the GBCD at different sintering temperatures.

II. Experimental Procedure

(1) Sample Preparation

Dense polycrystalline pellets of Y- and La-doped alumina at a doping level of 450 ppm and Y + La codoped alumina at a total doping level of 450 ppm were prepared with an ultra-pure -alumina powder (AA04; Sumitomo, Osaka, Japan) and pulsed electric current sintering, also commonly referred to as SPS. The powder preparation and SPS procedures are described in detail elsewhere.[25] For this work, the Y-, La-, and Y + La-doped samples were sintered at 1450°C, 1500°C, and 1600°C with a heating rate of 100°C/min and dwell times and sintering pressures as summarized in Table I. The resulting sample pieces were then polished by a series of diamond lapping films down to a surface roughness of 1 μm, with a subsequent final polishing step using an oxide polishing solution of silica to form the mirror-like surface needed for EBSD measurements. Note that all the sintered samples were sufficiently dense to show transparency or translucency depending on their grain sizes.[26] The changes in the sintering pressures and dwell times served the purpose of promoting grain growth and/or rendering the grain sizes comparable among the samples.

Table I. Summary of Processing Parameters used in the Sample Preparation

Dopants	Sintering temperature (°C)	Sintering pressure (MPa)	Dwell time (min)
Y	1450	100	1
Y	1500	100	3
Y	1600	100	3
La	1450	100	1
La	1500	50	3
La	1600	50	3
Y + La	1450	100	2
Y + La	1500	50	3
Y + La	1600	50	3

(2) Microstructure Characterization by EBSD

EBSD maps were collected for 450 ppm La-doped alumina sintered at 1500°C and 1600°C, 450 ppm Y-doped alumina sintered at 1450°C, 1500°C, and 1600°C, and 450 ppm La and Y codoped alumina sintered at 1500°C and 1600°C. The step size for each EBSD map, listed in Table II, was one-tenth the average grain size, such that the average length of the grain-boundary line segments was greater than four steps per line segment. Each map was cleaned up in the TSL software[27] to remove unindexed points using a single iteration grain dilation with a minimum grain size of three to five pixels/grain and a tolerance angle of 5°. The resulting grains were then assigned a single average orientation. Multiple grains in each scan had assigned orientations that were influenced by the so-called "pseudo-symmetry" problem, where the EBSD pattern recognition software could not distinguish between two similar orientations separated by particular rotations about symmetry axes, resulting in a low average confidence for the affected areas. This causes many false grain boundaries, obvious in orientation maps, such as the one shown in Fig. 1(a), that influence the misorientation distributions. In the present case, the false boundaries were mostly 30° or 60° rotations about [0001]. To remove the orientations introduced by pseudosymmetry, a grain confidence index (CI) standardization was applied, and an average CI partition was set, where the minimum grain size is two pixels, the minimum CI is 0.4, and the partition is set to only show grains with a CI greater than 0.4. This partition depends on scan quality, so poorer quality scans require a lower confidence index partition. By careful inspection of many orientation maps, it was ascertained that this procedure removes all false boundaries as well as areas obscured by contamination, leaving only true grain boundaries to be analyzed.

It should be noted that the built-in pseudosymmetry cleanup method in the TSL software removes all boundaries according to a misorientation criterion. When implemented here, it removed not only those introduced by the pseudosymmetry problem, but also true boundaries with the same misorientation, producing gaps in the misorientation distribution at these angles. We further note that we attempted to remove the false boundaries using geometric filters such as a minimum grain-boundary segment length criterion, increasing the minimum grain size to 20 pixels, and analysis of the tortuosity and connectivity of grain-boundary segments. However, none of these methods removed only the false boundaries introduced by the pseudosymmetry problem.

Figure 1 illustrates both the effects of pseudosymmetry on grain-boundary maps for a representative microstructure, the

Table II. Electron Backscatter Diffraction and Cleanup Parameters and Results

Dopant (ppm)	SPS temp. (°C)	Step size (μm)	Cleanup† (%)	Steps/segment‡	Line count‡
Y	1450	0.09	12.5	7.3	44,818
Y	1500	0.2	9.1	6.9	238,968
Y	1600	1.3	6.9	8.5	49,420
La	1500	0.5	10.0	6.7	325,425
La	1600	1.5	9.6	4.9	60,476
Y + La	1500	1.4	5.2	7.0	62,314
Y + La	1600	2.3	9.5	5.7	43,305

†Percent of data changed was before the CI standardization and corresponding partition.

‡Steps/segment and line count collected after pseudosymmetry cleanup.

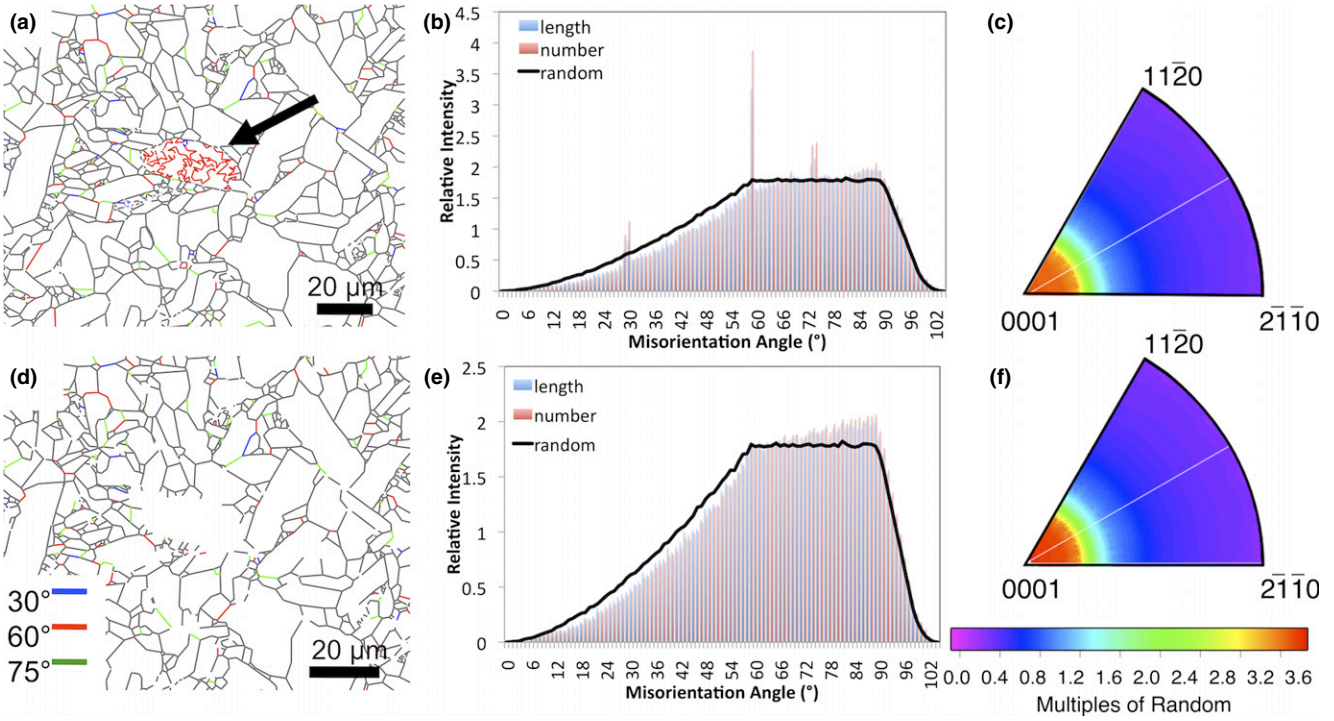

Fig. 1. Effect of pseudosymmetry on grain-boundary distributions in La-doped alumina sintered at 1500°C. Reconstructed line segments before clean up where red/blue/green lines show pseudosymmetry orientations (a), the corresponding one-dimensional misorientation distribution where the red bars are binned by grain-boundary line count, the blue bars represent line length weighted distributions, and the black line represents a simulated random distribution (b) and grain-boundary plane distribution in the crystal reference frame (c). Post cleanup line segment reconstruction showing removed pseudosymmetry (d), the corresponding misorientation distribution (e), and planar distributions (f).

misorientation distribution, and the grain-boundary plane distribution, as well as its removal using the CI partition method described above. In the grain-boundary map in Fig. 1(a), boundaries with misorientations of 30°, 60°, and 75° are colored blue, red, and green, respectively. Most of the boundaries are clearly part of the true grain-boundary network. However, boundaries that result from the pseudosymmetry effect are also found in tortuous paths within apparent grains (see area marked by arrow). Such boundaries always have one of the special misorientations and can create peaks in the distribution of grain boundaries as a function of misorientation angle [Fig. 1(b)]. After the pseudosymmetry cleanup procedure described above, the false boundaries in Fig. 1(a) are removed and the real boundaries are preserved [see Fig. 1(d)]. Furthermore, when the misorientation distribution is recalculated [see Fig. 1(e)], the artificial peaks produced by the false boundaries are no longer found. Note that because of the random orientations of the false pseudosymmetry boundary planes, the planar distributions [Figs. 1(c) and (f)] are not significantly influenced.

After the clean up, the grain-boundary line segments were extracted using the TSL software. The acquisition of several hundred thousand grain-boundary line segments for the 450 ppm Y-doped and 450 ppm La-doped aluminas sintered at 1500°C made it possible to calculate the five-parameter GBCDs at misorientations where the population is higher than random. For the other samples, only the distribution of grain-boundary planes in the crystal reference frame, independent of misorientation, was calculated. The GBCD calculations, which use the stereological relationship between line length per area and area per volume, were carried out using a modified version of calc_gbcd_stereo.[22,24] The program discretizes the grain-boundary parameters and, in the original version of the program that was used in previous studies, the domain of Euler angles was limited to angles between 0° and 90°. This is acceptable for higher symmetry materials, but is a fraction of a single fundamental zone for trigonal materials. To accommodate the trigonal symmetry, we used a domain that contains the full range of possible Euler angles, discretized into bins ~10° wide. In the calculations, we used the symmetry operators of point group 32, because this is the rotation group of alumina's $\bar{3}m$ Laue group.

III. Results

Figures 2–4 show representative grain orientation maps for all seven samples. From these maps, it is possible to comment on the effect of sintering time and dopant on the microstructural development of alumina. La-doped alumina sintered at 1500°C shows a high aspect ratio grain morphology and normal grain growth, as seen in Fig. 2(a). Figure 2(b) shows La-doped alumina sintered at 1600°C, exhibiting the same elongated grain growth and a larger, yet still unimodal, grain size.

Y-doped alumina sintered at 1450°C displayed an equiaxed grain morphology and normal grain growth, as seen in Fig. 3(a). When the sintering temperature was increased to 1500°C, the microstructure consisted of both small and very large equiaxed grains—indicating AGG [see Fig. 3(b)]. When sintered at 1600°C, the faster growing grains impinge to form a coarser grained microstructure, shown in Fig. 3(c).

Y + La codoped alumina sintered at 1500°C and 1600°C both displayed an equiaxed grain morphology and normal grain growth, as illustrated in Figs. 4(a) and (b). The microstructures exhibit characteristics of both the Y and La singly doped samples. Similar to the Y-doped samples, the microstructures have an equiaxed grain morphology, and similar to the La-doped microstructures, the grain growth is normal at 1600°C.

The distributions of grain-boundary planes, independent of misorientation, were calculated for each sample. The distributions for La-doped alumina at 1500°C and 1600°C are shown in Figs. 5(a) and (b), respectively. It was found that both the 1500°C and 1600°C La-doped alumina samples showed a significant preference for (0001) planes. The 1600°C sample shows a 15% decrease in the relative popula-

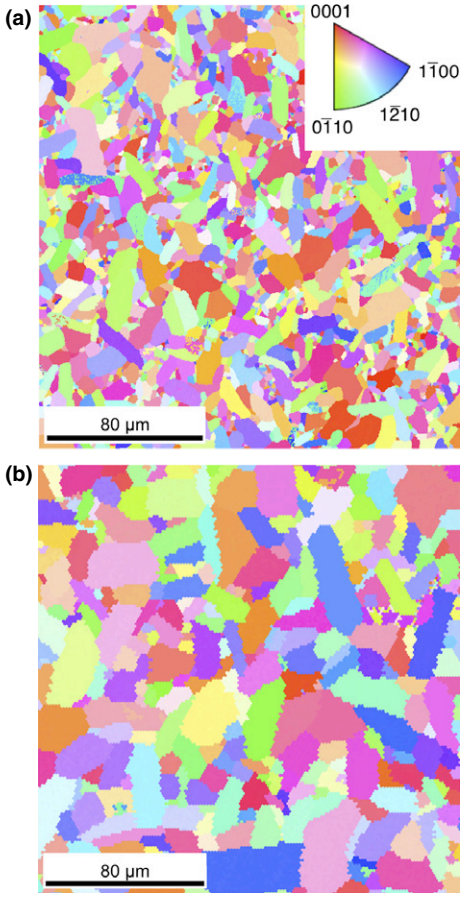

Fig. 2. Orientation maps of 450 ppm La-doped alumina (a) SPS temperature 1500°C and (b) SPS temperature of 1600°C. Images from before pseudosymmetry cleanup.

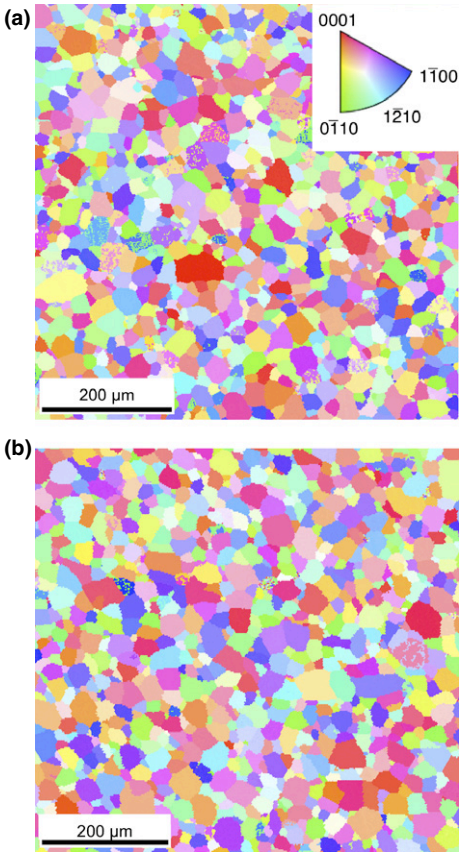

Fig. 4. Orientation maps of 450 ppm Y- and La-codoped alumina at (a) 1500°C and (b) 1600°C. Images from before pseudosymmetry cleanup.

tion of (0001) planes, suggesting that as the temperature increases, the distribution becomes less anisotropic.

The distribution of grain-boundary planes, independent of misorientation, in the Y-doped alumina samples sintered at 1450°C [Fig. 6(a)] showed a random distribution of grain-boundary planes. The sample sintered at 1500°C [Fig. 6(b)], which had a bimodal grain size distribution, had a preference for grain-boundary planes with the $\{01\bar{1}2\}$ orientation, referred to as the *R* plane. In the impinged microstructure, sintered at 1600°C, the preference was for grain-boundary planes with the $\{11\bar{2}0\}$ orientation [Fig. 6(c)], referred to as the A plane. Note that the widths of these distributions are much narrower than the La-doped samples.

Finally, the grain-boundary plane distribution for the Y + La codoped alumina is shown in Fig. 7. This distribution has a preference for (0001) and $\{01\bar{1}2\}$ oriented grain-boundary planes, as well the orientations between these planes. Furthermore, the distribution was approximately the same at 1600°C. This suggests that La suppresses the transition in grain-boundary mobility that is found in the Y-doped sample at 1500°C.

The grain-boundary misorientation distribution was calculated with the same EBSD-derived line segments used for the GBCD calculations. Note that a large amount of data was used for these calculations, as seen under the total line segments analyzed in Table II, and that these distributions are representative of the entire analyzed microstructure, rather than a single field of view. Previously reported misorientation distributions had fewer observations and were therefore

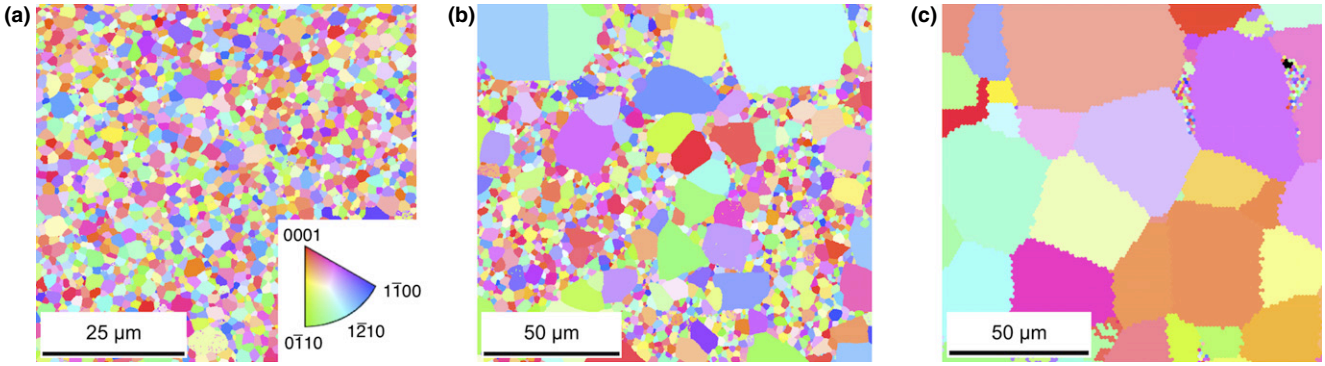

Fig. 3. Orientation maps of 450 ppm Y-doped alumina with an SPS temperature of (a) 1450°C, (b) 1500°C, and (c) 1600°C. The scale bar for (a) is 25 μm whereas in (b) and (c) the scale bars are 50 μm. Images from before pseudosymmetry cleanup.

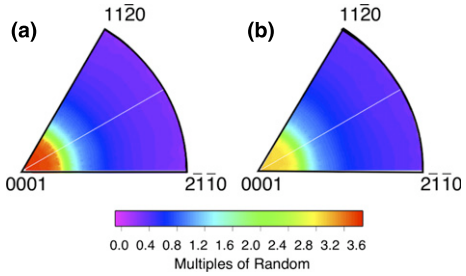

Fig. 5. Grain-boundary plane distributions, independent of misorientation, plotted in stereographic projection with the $(2\bar{1}\bar{1}0)$ plane orientated horizontally to the right and the (0001) plane normal to the figure. Subsequent figures are plotted the same way. La-doped alumina sintered at (a) 1500°C, and (b) 1600°C.

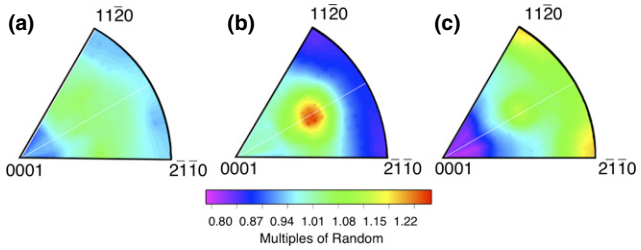

Fig. 6. The distribution of grain-boundary planes, independent of misorientation, in Y-doped alumina after heating at (a) 1450°C, (b) 1500°C, and (c) 1600°C.

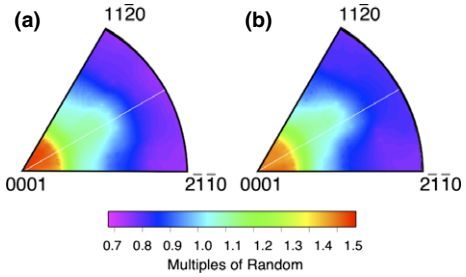

Fig. 7. Distribution of grain-boundary planes, independent of misorientation, for Y + La codoped samples sintered at (a) 1500°C and (b) 1600°C.

classified into bins with a wider angular range. The earlier work showed a general trend for slightly higher populations of boundaries with misorientations near 30°, 60°, and 90°.[13,28] The current work, with many more boundary observations, uses a finer (1°) discretization and is still able to produce smooth distributions. In addition, because false boundaries related to pseudosymmetry have been removed, we can have confidence that nonrandom features in the distribution are meaningful.

The distributions of grain-boundary misorientations depend on the dopant as well as grain growth kinetics. The Y-doped alumina samples show an increasing population of 60° boundaries with increasing sintering temperatures and increasing population of high mobility boundaries. This is illustrated in Fig. 8, where the distributions of all grain-boundary misorientations are compared with grain-boundary maps of subsets of the data with 60° misorientations highlighted. After calculating the three-parameter misorientation distribution function (not shown), it was concluded that the peak at 60° corresponded to 60°/[0001] misorientation which is the Σ3 boundary in the alumina system. A large population of what appear to be twin boundaries [highlighted in red in Fig. 8(c)] appears after the impingement of the large, fast-growing grains in the Y-doped alumina sample sintered at 1600°C. The La-doped alumina samples, one of which can be seen in Fig. 1, do not exhibit the same trend and there are no significant deviations from the random distribution. The Y + La codoped samples exhibit a consistently high population of 60° misorientation boundaries where the maximum peak relative intensity is between that of the 1500°C and 1600°C Y-doped samples. This allows us to conclude that while the Y + La codoping did not exhibit AGG at the tested sintering temperatures, the increased population of 60° misorientations indicates a misorientation dependence similar to Y-doped samples that exhibit AGG.

The distribution of grain-boundary planes for the Σ3, or 60°/[0001] boundaries for Y- and La-doped alumina sintered at 1500°C are shown in Fig. 9. There is a preference for $\{01\bar{1}2\}$ orientations in Y-doped alumina and for (0001) orientations in La-doped alumina, which is consistent with the two-parameter grain-boundary plane distributions shown in Figs. 5 and 6. For the case of the 60°/[0001] boundary in the Y-doped sample [Fig. 9(a)], the relative areas of the $\{01\bar{1}2\}$ orientations are 50% greater than random. In the distribution for the La-doped sample [Fig. 9(b)], the maximum is ~3.2 MRD. Based on the data in Fig. 8(b), one might expect this to be larger. However, the relatively large bin size used for the five-parameter calculation (10°) effectively smoothes the maximum in the one-parameter misorientation distribution.

IV. Discussion

The current results provide a comprehensive description of the GBCD in Y- and La-doped alumina. Previous research has concluded that during normal grain growth, the GBCD reaches an approximate steady state that is insensitive to average grain size.[29,30] This is consistent with the observations in the La-doped and Y + La codoped alumina, shown in Figs. 5 and 7, that show only minor changes with grain growth. However, when AGG occurs in the Y-doped alumina,[7] there is a significant change in the GBCD. This is also consistent with observations in other doped aluminas and in Ca-doped yttria.[31,32] This change in the grain-boundary plane distribution has been connected to changes in the grain-boundary energies, which tend to decrease for complexions with increasing concentrations of solute.[19,32] Similarly, the misorientation angle preference in the case of AGG caused by the complexion transition shows a distinct increase in 60° misorientations as well as a change in the preferences for the orientations of grain-boundary planes. However, with normal grain growth in the La- and Y + La codoped samples, the misorientation distribution is constant as well as the distribution of boundary planes. The observation that the GBCD is sensitive to dopants is consistent with the conclusions from a study of doped magnesia.[33] This understanding of the relationship between doping elements, grain growth kinetics, and grain-boundary character development, if predictable, could lead to new insights into ceramic grain-boundary engineering. At the same time, we must also note that the mesoscale results presented here do not allow us to be certain about the atomic scale structure and composition of the interfaces in these materials.

The previous studies of the effect of complexion transitions on grain-boundary plane distributions only considered the distributions before and during the transition; here we also have data after the transition.[31,32] The distribution of planes during the expansion of the fast-growing grains into the smaller grains is dominated by $\{01\bar{1}2\}$ planes, but after the grains impinge, $\{11\bar{2}0\}$ -type planes are preferred. In the absence of AGG, the relative grain-boundary energies are the most important factors that influence the grain-boundary population.[29,34] Therefore, the observations indicate that after the complexion transition, the boundaries terminated on $\{11\bar{2}0\}$ -type planes have relatively lower energies. However, in the transient growth stage, the boundaries around

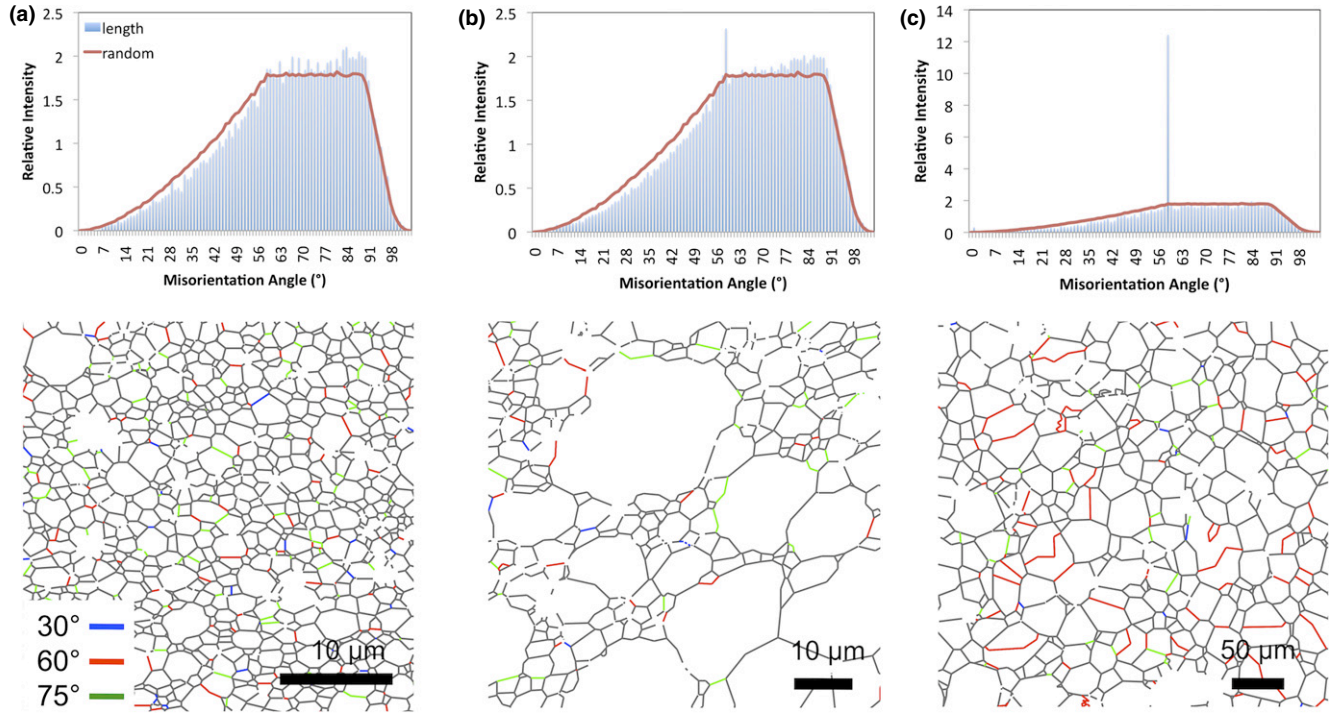

Fig. 8. Misorientation distributions and corresponding reconstructed grain-boundary line segments for Y-doped alumina sintered at 1450°C (a), 1500°C (b), and 1600°C—exhibiting a large increase in 60° boundaries (c). Based on the configuration of the 60° boundaries, it is concluded that they do not result from incorrect indexing because of pseudosymmetry. Misorientation angle distribution bin sizes are 1° and range from 0° to 104°.

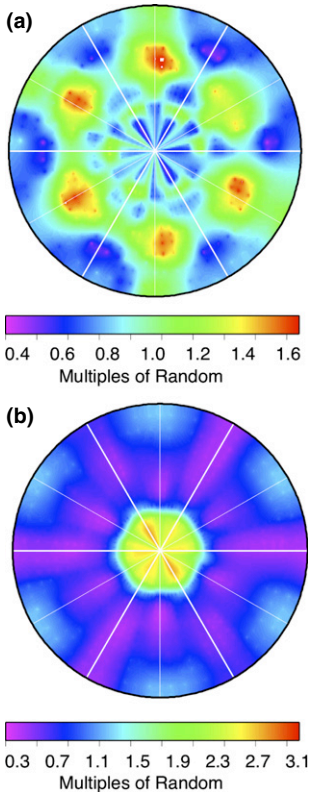

Fig. 9. The grain-boundary plane distribution in Y-doped alumina sintered at 1500°C at a 60°/[0001] misorientation (a) and in La-doped alumina sintered at 1500°C at a 60°/[0001] (b).

the large abnormal grains will dominate the population, and the orientation of these boundaries is more likely to be determined by relative mobilities.

It should be noted that the grain-boundary orientation distribution in the Y-doped alumina system is not strongly anisotropic. The relative areas of the preferred grain-boundary planes are only about 1.3 times more likely to occur than an orientation in a random distribution. The more important nonrandom characteristic of the grain-boundary distribution is found in the domain of misorientations, with a strong preference for the Σ3 grain boundary (see Fig. 8). There is ample experimental and theoretical evidence that as grain growth occurs, the lowest energy boundaries are eliminated less frequently and accumulate in the network.[35] This is one possible explanation of the increase in Σ3 grain boundaries with grain growth. However, it is also possible another mechanism generates these twins. It should also be noted that the La- and Y + La-doped alumina show a strong preference for (0001) grain-boundary plane orientations, regardless of misorientation.

Galmarini *et al.*[36] simulated the effect of Y segregation on the energies of alumina surfaces and grain boundaries. From these calculations, it was determined that Y segregated to $\{11\bar{2}0\}$ and $\{01\bar{1}2\}$ surfaces at 1600°C, with the $\{11\bar{2}0\}$ plane having its relative energy decreased the most. The energies of selected low Σ-Coincident Site Lattice (CSL) boundaries with and without Y were also calculated. The results showed that Y segregated to some, but not all boundaries, and also lowered the energy. With limited numbers of calculations, it is not possible to make detailed comparisons to the present work. However, we can remark that Galmarini's prediction that for the Σ3 boundaries, $\{11\bar{2}0\}$ plane grain boundaries in Y-doped alumina are much lower in energy than the (0001) plane boundaries is consistent with the observed populations.

Experimentally, Gülgün *et al.*[8] observed a high proportion of (0001), $\{11\bar{2}0\}$, and $\{01\bar{1}2\}$ plane interfaces in the Y-doped alumina samples they investigated using transmission electron microscopy (TEM). Similarly, another TEM study, reported by Bouchet *et al.*,[20] showed that Y-doped alumina sintered at 1450°C and 1550°C both showed a higher level of Y segregation to the $\{01\bar{1}2\}$ -plane than to (0001); in their study, the Y/Al intensity peak ratio for $\{01\bar{1}2\}$ planes was 2.5–2.7 compared to 0.2–1.7 for (0001) planes. Both of these investigations are consistent with the

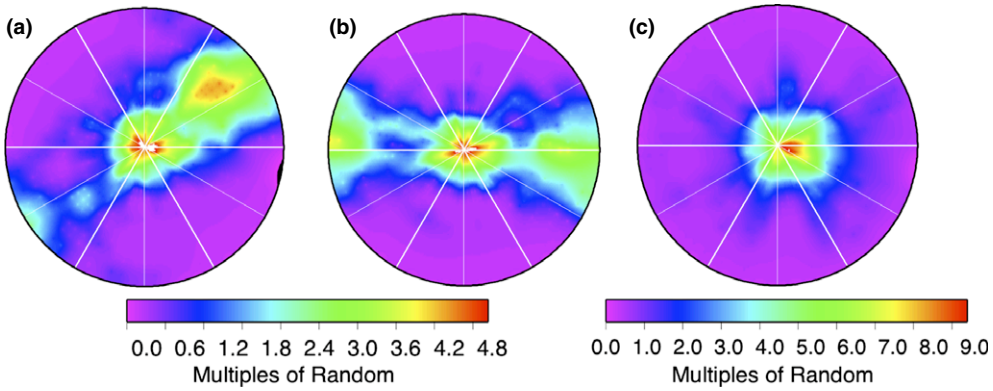

Fig. 10. Grain-boundary plane distributions for La-doped alumina sintered at 1600°C. (a) $\Sigma 7_a G$ (85.9°/[02$\bar{2}$1]), (b) $\Sigma 7_2 V$ (85.9°/[24$\bar{6}$1]), (c) $\Sigma 31_b G$ (63.15°/[11$\bar{2}$3]).

current mesoscale experimental results that at temperatures above 1450°C, Y segregation leads to a complexion transition that lowers the energy of boundaries with {01$\bar{1}$2} planes and increases the grain-boundary mobility. When the transition occurs only around some grains, AGG results. After the fast-growing grains impinge, the {11$\bar{2}$0} plane is the most common, suggesting that this orientation has the lowest energy.

There have been several mesoscale studies of grain-boundary populations in alumina. In general, no large-scale deviations from random misorientation distributions have been found in pure or doped aluminas.[13,21,28] Furthermore, the populations of low Σ-CSLs are only modestly enhanced in population over the population expected in a random distribution. For example, Vonlanthen and Grobety[28] found that about 4% of the boundaries in alumina could be classified as belonging to a CSL misorientation with $\Sigma \leq 28$, compared to an expectation of 2.7% in a random distribution. Cho *et al.*[13] reported that Y doping increased the occurrence of Σ3 boundaries from roughly 0.6% to 2.3%. The observed increase that occurs with Y doping is consistent with this study.

While it has been shown that lattice coincidence is not a good predictor of the relative population or energies of the grain boundaries,[34,37] the use of CSL notation is convenient when trying to compare results from different analysis techniques, and is prevalent in alumina grain-boundary research. However, this literature is not entirely consistent in nomenclature. The first list of CSL misorientations for rhombohedral α-alumina was published by Grimmer *et al.*[38] More recently, Vonlanthen and Grobety,[28] beginning from Grimmer's previous report on coincident orientations in rhombohedral materials,[39] accounted for the possibility of small variations in the *c*/*a* ratio and in some cases reached different results for alumina. So that there is no confusion, the source of the specified notation and misorientation will be labeled in each case with a "G" Grimmer *et al.*[38] or a "V" for Vonlanthen and Grobety.[28]

Figure 10 shows the distribution of grain-boundary planes for the $\Sigma 7_a$(G), $\Sigma 7_2$(V), and $\Sigma 31_b$(G) boundaries in La-doped alumina sintered at 1500°C. In each case, the maximum is near (0001), indicating a preference for the basal plane. This is consistent with the results in Fig. 5 that are averaged over all misorientations. It should be noted from the grain-boundary plane distributions that these misorientations are not significantly different from those at randomly selected misorientations. This leads us to conclude that lattice coincidence does not impart any special significance to these boundaries. Similar plots for the Y-doped system (not shown) did not show strong maxima or other characteristics that distinguished them as special. However, we also note that at the current resolution of ~10°, there is a possibility that a special boundary that occurs in a very narrow angular range will be averaged with neighboring boundaries such that its apparent population is less than its true population. It is currently not possible to examine plane distributions at specific misorientations at higher resolution, because of the size of the domain of boundary types.

Bicrystal Symmetric Tilts

The grain-boundary energies of symmetric tilt boundaries have been experimentally evaluated using bicyrstals,[40–43] calculated by static lattice simulations,[44] and density functional theory.[45] Kenway[44] calculated the grain-boundary energy of the {10$\bar{1}$1}/{101$\bar{1}$} tilt with a near Σ11 misorientation, the boundary was tilted 144.8° around $<1\bar{2}10>$. Milas *et al.*[45] further modeled the same near Σ11 boundary to explore the grain-boundary structure with the addition of transition metals, such as Y. Here, we look at experimental measurements of bulk alumina to determine the likelihood of grain boundaries with these misorientations occurring in a real sample. The Y-doped alumina GBCD for 144.8°/[1$\bar{2}$10] shows a strong population of ($\bar{1}$01$\bar{1}$), (0001), and (10$\bar{1}$0) planes along the tilt axis [Fig. 11(a)]. While the expected {10$\bar{1}$1}/{101$\bar{1}$} planes did occur, they are not the only tilt boundaries at the specified misorientation. The La-doped GBCD of the near Σ11 boundary shows a high population of (0001) planes with no tilt boundary preference. However, a real $\Sigma 11_b$(G) boundary at 95.2°/[01$\bar{1}$0] in La-doped alumina reveals a tilt boundary of (0001) and a geometrically necessary complement of ($\bar{2}$110) planes [Fig. 11(b)]. Note that this preference for the basal orientation on one side of the boundary is a characteristic at all tilt angles.

Nishimura *et al.*[40] investigated the atomic structures and energies of Σ7 (38.2°/[0001]) symmetric tilt boundary bicrystals with grain-boundary planes {4$\bar{5}$10}, {2$\bar{3}$10}, and {1$\bar{1}$02}. While the chemistry of these samples is not the same, this is the only prior work available for comparison in which all five crystallographic parameters of the measured grain boundaries were controlled. It was found that the {1$\bar{1}$02} plane exhibited the lowest grain-boundary energy, and concluded that the grain-boundary energy is highly dependent on the grain-boundary plane. Figures 12(a) and (b) show the Σ7 boundary in the Y-doped and La-doped alumina samples, respectively. The Y-doped sample shows a weak preference for {1$\bar{1}$02} planes and this suggests that it is the lowest energy grain-boundary plane, consistent with the findings of Nishimura *et al.*[40] The La-doped sample shows a preference for the (0001) twist boundaries. The lack of agreement in this case is not surprising considering that the grain-boundary chemistry differs and this can alter the grain-boundary energies.

Conclusions

While Y and La doping both increase the creep resistance in alumina, they have different grain-boundary plane and misorientation distributions. After false boundaries that derive

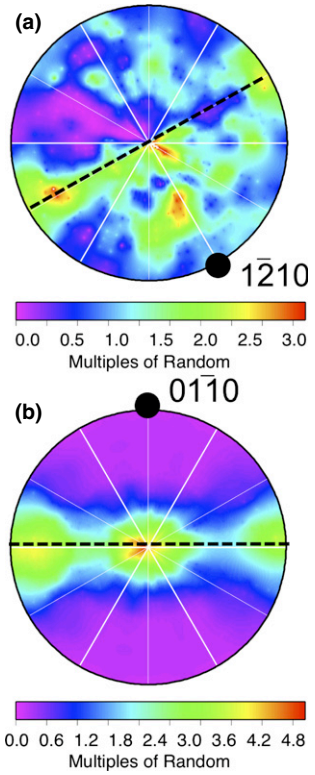

Fig. 11. The grain-boundary plane distribution for boundaries with a misorientation of 144.2°/[$1\bar{2}10$] (near Σ11) of Y-doped alumina, showing ($\bar{1}01\bar{1}$), (0001), and ($10\bar{1}0$) planes oriented along the tilt zone (a). The misorientation axis and tilt zone are defined by black circle and dotted line, respectively. The grain-boundary plane distribution for boundaries with a misorientation of 95.2°/[$01\bar{1}0$] ($\Sigma 11_b$) of La-doped alumina showing a symmetric boundary with high populations at (0001) and ($\bar{2}110$) planes—both of which are oriented along the [$01\bar{1}0$] tilt axis (b).

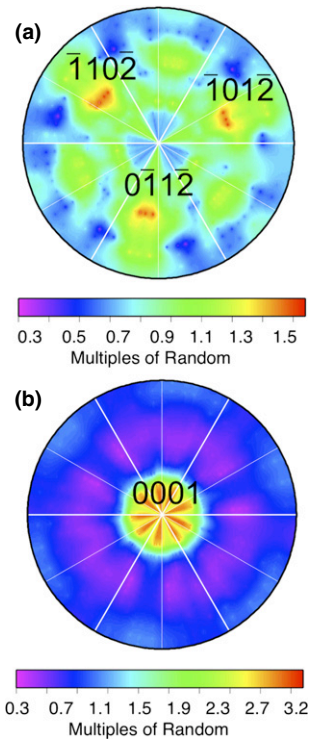

Fig. 12. Distribution of grain-boundary planes for the misorientation of 38.2°/[0001] (Σ7) for (a) Y-doped alumina and (b) La-doped alumina.

from pseudosymmetry effects are removed, the misorientation distribution in La-doped alumina is essentially random. However, the grain boundaries do show a preference for (0001) planes at all temperatures and at all misorientations. At 1500°C, the preference is, on average, 3.7 times random. Y-doped alumina, on the other hand, has a larger than random population of Σ3 grain boundaries, with a 60° misorientation about the [0001] axis. After annealing at 1600°C, these boundaries occur in the population six times more than expected in a random distribution. With that one exception, other low Σ CSL boundaries had no characteristics to distinguish them from random boundaries in any of the samples. Y-doped alumina undergoes a complexion transition between 1450°C and 1600°C in which higher mobility grain boundaries appear, leading to AGG. The Y-doped materials have a preference for {$01\bar{1}2$} -planes during AGG and {$11\bar{2}0$} -planes after the abnormal grains impinge. Y + La-codoping results in a microstructure consisting of equiaxed grains that exhibit both a preference for (0001) and {$01\bar{1}2$} orientations.

Acknowledgment

Financial support provided by the ONR-MURI under the grant no. N00014-11-1-0678 and the Swiss National Science Foundation under grant no. 200021-122288/1 are gratefully acknowledged. Support for facilities by the MRSEC program of the National Science Foundation under award DMR- 0520425 is also acknowledged.

References

[1]J. Cho, M. P. Harmer, H. M. Chan, J. M. Rickman, and A. M. Thompson, "Effect of Yttrium and Lanthanum on the Tensile Creep Behavior of Aluminum Oxide," *J. Am. Ceram. Soc.*, **80** [4] 1013–7 (1997).

[2]J. P. Buban, K. Matsunaga, J. Chen, N. Shibata, W. Y. Ching, T. Yamamoto, and Y. Ikuhara, "Grain Boundary Strengthening in Alumina by Rare Earth Impurities," *Science*, **311** [5758] 212–5 (2006).

[3]S. Lartigue-Korinek, C. Carry, and L. Priester, "Multiscale Aspects of the Influence of Yttrium on Microstructure, Sintering and Creep of Alumina," *J. Eur. Ceram. Soc.*, **22** [9–10] 1525–41 (2002).

[4]K. Matsunaga, H. Nishimura, H. Muto, T. Yamamoto, and Y. Ikuhara, "Direct Measurements of Grain Boundary Sliding in Yttrium-Doped Alumina Bicrystals," *Appl. Phys. Lett.*, **82** [8] 1179–81 (2003).

[5]H. Yoshida, Y. Ikuhara, and T. Sakuma, "High-Temperature Creep Resistance in Rare-Earth-Doped, Fine-Grained Al_2O_3," *J. Mater. Res.*, **13** [9] 2597–601 (1998).

[6]A. M. Thompson, K. K. Soni, H. M. Chan, M. P. Harmer, D. B. Williams, J. M. Chabala, and R. Levi-Setti, "Dopant Distributions in Rare-Earth-Doped Alumina," *J. Am. Ceram. Soc.*, **80** [2] 373–6 (1997).

[7]C. M. Wang, G. S. Cargill III, H. M. Chan, and M. P. Harmer, "Structural Features of Y-Saturated and Supersaturated Grain Boundaries in Alumina," *Acta Mater.*, **48** [10] 2579–91 (2000).

[8]M. A. Gülgün, V. Putlayev, and M. Rühle, "Effects of Yttrium Doping α-Alumina: I, Microstructure and Microchemistry," *J. Am. Ceram. Soc.*, **82** [7] 1849–56 (1999).

[9]J. Chen, L. Ouyang, and W. Y. Ching, "Molecular Dynamics Simulation of Y-Doped Sigma 37 Grain Boundary in Alumina," *Acta Mater.*, **53**, 4111–20 (2005).

[10]J. Chen, Y.-N. Xu, P. Rulis, L. Ouyang, and W.-Y. Ching, "*Ab Initio* Theoretical Tensile Test on Y-Doped Sigma = 3 Grain Boundary in alpha-Al_2O_3," *Acta Mater.*, **53**, 403–10 (2004).

[11]R. Voytovych, I. MacLaren, M. A. Gulgun, R. M. Cannon, and M. Rühle, "The Effect of Yttrium on Densification and Grain Growth in α-Alumina," *Acta Mater.*, **50**, 3453–63 (2002).

[12]I. MacLaren, R. M. Cannon, M. A. Gülgün, R. Voytovych, N. Popescu-Pogrion, C. Scheu, U. Täffner, and M. Rühle, "Abnormal Grain Growth in Alumina: Synergistic Effects of Yttria and Silica," *J. Am. Ceram. Soc.*, **86** [4] 650–9 (2003).

[13]J. Cho, C. M. Wang, H. M. Chan, J. M. Rickman, and M. P. Harmer, "A Study of Grain-Boundary Structure in Rare-Earth Doped Aluminas Using an EBSD Technique," *J. Mater. Sci.*, **37** [1] 59–64 (2002).

[14]M. A. Gulgun, R. Voytovych, I. MacLaren, M. Ruhle, and R. M. Cannon, "Cation Segregation in an Oxide Ceramic with Low Solubility: Yttrium Doped α-Alumina," *Interface Sci.*, **10**, 99–110 (2002).

[15]P. R. Cantwell, M. Tang, S. J. Dillon, J. Luo, G. S. Rohrer, and M. P. Harmer, "Grain Boundary Complexions," *Acta Mater.*, (2013).

[16]J. Fang, M. Thompson, M. P. Harmer, and H. M. Chan, "Effect of Yttrium and Lanthanum on the Final-Stage Sintering Behavior of Ultrahigh-Purity Alumina," *J. Am. Ceram. Soc.*, **80** [8] 2005–12 (1997).

[17]S. J. Dillon and M. P. Harmer, "Demystifying the Role of Sintering Additives with "Complexion"," *J. Eur. Ceram. Soc.*, **28** [7] 1485–93 (2008).

[18]S. J. Dillon, M. Tang, W. C. Carter, and M. P. Harmer, "Complexion: A New Concept for Kinetic Engineering in Materials Science," *Acta Mater.*, **55** [18] 6208–18 (2007).

[19]S. J. Dillon, M. P. Harmer, and G. S. Rohrer, "The Relative Energies of Normally and Abnormally Growing Grain Boundaries in Alumina Displaying Different Complexions," *J. Am. Ceram. Soc.*, **93** [6] 1796–802 (2010).
[20]D. Bouchet, F. Dupau, and S. Lartigue-Korinek, "Structure and Chemistry of Grain Boundaries in Yttria Doped Aluminas," *Microsc. Microanal. Microstruct.*, **4** [6] 561–73 (1993).
[21]J. Cho, H. M. Chan, M. P. Harmer, and J. M. Rickman, "Influence of Yttrium Doping on Grain Misorientation in Aluminum Oxide," *J. Am. Ceram. Soc.*, **81** [11] 3001–4 (1998).
[22]G. S. Rohrer, "Index of/~Gr20/Stereology"; Vol. 2011, http://mimp.materials.cmu.edu/~gr20/stereology/130728_full_domain_stereology.zip, 2013.
[23]D. M. Saylor, B. S. El-Dasher, B. L. Adams, and G. S. Rohrer, "Measuring the Five-Parameter Grain-Boundary Distribution from Observations of Planar Sections," *Metall. Mater. Trans. A*, **35A** [7] 1981–9 (2004).
[24]D. M. Saylor and G. S. Rohrer, "Determining Crystal Habits from Observations of Planar Sections," *J. Am. Ceram. Soc.*, **85** [11] 2799–804 (2002).
[25]M. Stuer, Z. Zhao, U. Aschauer, and P. Bowen, "Transparent Polycrystalline Alumina Using Spark Plasma Sintering: Effect of Mg, Y and La Doping," *J. Eur. Ceram. Soc.*, **30** [6] 1335–43 (2010).
[26]M. Stuer, P. Bowen, M. Cantoni, C. Pecharroman, and Z. Zhao, "Nanopore Characterization and Optical Modeling of Transparent Polycrystalline Alumina," *Adv. Funct. Mater.*, **22** [11] 2303–9 (2012).
[27]EDAX-TSL, "EDAX-TSL OIM 6.1 EBSD"; Ametek, Mahwah, NJ, 2011.
[28]P. Vonlanthen and B. Grobety, "CSL Grain Boundary Distribution in Alumina and Zirconia Ceramics," *Ceram. Int.*, **34** [6] 1459–72 (2008).
[29]J. Gruber, D. C. George, A. P. Kuprat, G. S. Rohrer, and A. D. Rollett, "Effect of Anisotropic Grain Boundary Properties on Grain Boundary Plane Distributions during Grain Growth," *Scripta Mater.*, **53** [3] 351–5 (2005).
[30]H. M. Miller and G. S. Rohrer, "Evolution of the Grain Boundary Character Distribution in Strontium Titanate During Grain Growth"; pp. 335–42 in *Applications of Texture Analysis*. John Wiley & Sons, Inc., Hoboken, NJ, 2009.
[31]S. J. Dillon, H. Miller, M. P. Harmer, and G. S. Rohrer, "Grain Boundary Plane Distributions in Aluminas Evolving by Normal and Abnormal Grain Growth and Displaying Different Complexions," *Int. J. Mater. Res.*, **101** [1] 50–6 (2010).
[32]S. A. Bojarski, S. Ma, W. Lenthe, M. P. Harmer, and G. S. Rohrer, "Changes in the Grain Boundary Character and Energy Distributions Resulting From a Complexion Transition in Ca-Doped Yttria," *Metall. Mater. Trans. A*, **43A**, 3532–8 (2012).
[33]F. Papillon, G. S. Rohrer, and P. Wynblatt, "Effect of Segregating Impurities on the Grain-Boundary Character Distribution of Magnesium Oxide," *J. Am. Ceram. Soc.*, **92** [12] 3044–51 (2009).
[34]G. S. Rohrer, "Grain Boundary Energy Anisotropy: A Review," *J. Mater. Sci.*, **46**, 2881–5895 (2011).
[35]S. J. Dillon and G. S. Rohrer, "Mechanism for the Development of Anisotropic Grain Boundary Character Distributions During Normal Grain Growth," *Acta Mater.*, **57**, 1–7 (2009).
[36]S. Galmarini, U. Aschauer, P. Bowen, and S. C. Parker, "Atomistic Simulation of Y-Doped α-Alumina Interfaces," *J. Am. Ceram. Soc.*, **91** [11] 3643–51 (2008).
[37]D. M. Saylor, B. S. El Dasher, A. D. Rollett, and G. S. Rohrer, "Distribution of Grain Boundaries in Aluminum as a Function of Five Macroscopic Parameters," *Acta Mater.*, **52** [12] 3649–55 (2004).
[38]H. Grimmer, R. Bonnet, S. Lartigue, and L. Priester, "Theoretical and Experimental Descriptions of Grain Boundaries in Rhombohedral α-Al_2O_3," *Philos. Mag. A*, **61** [3] 493–509 (1990).
[39]H. Grimmer, "Coincidence Orientations of Grains in Rhombohedral Materials," *Acta Crystallogr. Sect. A*, **45**, 505–23 (1989).
[40]H. Nishimura, K. Matsunaga, T. Saito, T. Yamamoto, and Y. Ikuhara, "Atomic Structures and Energies of Σ7 Symmetrical Tilt Grain Boundaries in Alumina Bicrystals," *J. Am. Ceram. Soc.*, **86** [4] 574–80 (2003).
[41]J. F. Shackelford and W. D. Scott, "Relative Energies of (1100) Tilt Boundaries in Aluminum Oxide," *J. Am. Ceram. Soc.*, **51** [12] 688–92 (1968).
[42]T. Hoche, P. R. Kenway, H.-J. Kleebe, and M. Rühle, "High-Resolution Transmission Electron Microscopy Studies of a Near Σ11 Grain Boundary in α-Alumina," *J. Am. Ceram. Soc.*, **77** [2] 339–48 (1994).
[43]T. Gemming, S. Nufer, W. Kurtz, and M. Rühle, "Structure and Chemistry of Symmetrical Tilt Grain Boundaries in α-Al_2O_3: II, Bicrystals with Y at the Interface," *J. Am. Ceram. Soc.*, **86** [4] 590–4 (2003).
[44]P. R. Kenway, "Calculated Structures and Energies of Grain Boundaries in Alpha-Al_2O_3," *J. Am. Ceram. Soc.*, **77** [2] 349–55 (1994).
[45]I. Milas, B. Hinnemann, and E. A. Carter, "Structure of and Ion Segregation to an Alumina Grain Boundary: Implications for Growth and Creep," *J. Mater. Res.*, **23** [5] 1494–508 (2008). □